Phase structure of the anisotropic antiferromagnetic Heisenberg model on a layered triangular lattice: Spiral state and deconfined spin liquid

Kazuya Nakane, Takeshi Kamijo,* and Ikuo Ichinose
Department of Applied Physics, Nagoya Institute of Technology, Nagoya 466-8555 Japan
(Received 29 September 2010; revised manuscript received 6 December 2010; published 11 February 2011)

In the present paper, we study a spin-1/2 antiferromagnetic (AF) Heisenberg model on layered anisotropic triangular lattice and obtain its phase structure. We use the Schwinger bosons for representing spin operators and also a coherent-state path integral for calculating physical quantities. Finite-temperature properties of the system are investigated by means of the numerical Monte-Carlo simulations. A detailed phase diagram of the system is obtained by calculating internal energy, specific heat, spin correlation functions, etc. There are AF Néel, paramagnetic, and spiral states. Turning on the plaquette term (i.e., the Maxwell term on a lattice) of an emergent U(1) gauge field that flips a pair of parallel spin-singlet bonds, we found that there appears a phase that is regarded as a deconfined spin-liquid state, though "transition" to this phase from the paramagnetic phase is not of second order but a crossover. In that phase, the emergent gauge boson is a physical gapless excitation coupled with spinons. These results support our previous study on an AF Heisenberg model on a triangular lattice at vanishing temperature.

DOI: 10.1103/PhysRevB.83.054414 PACS number(s): 75.50.Ee, 11.15.−q, 75.10.Jm

I. INTRODUCTION

The study of quantum spin models has a long history. In particular after the discovery of the high-temperature superconductors, exotic quantum spin states have been intensively explored. Among them, the spin-liquid state with a deconfined spinon has interested many theoretical and experimental researchers.[1] Recently, experiments of the layered anisotropic triangular antiferromagnet (AF magnet) Cs_2CuCl_4 revealed the existence of the incommensurate spiral order at low temperature (T) and also spinonlike excitations at intermediate T.[2,3] One may think that this material can be a candidate for so-called Z_2 spin liquid.[4] Furthermore, very recently, evidence for a spin liquid in a layered anisotropic triangular AF magnet $EtMe_3Sb[Pd(dmit)_2]_2$ at very low T has been reported.[5]

In the previous paper,[6] we studied a frustrated AF Heisenberg model on an anisotropic triangular lattice in two dimensions (2D) at $T = 0$. We used the Schwinger bosons for representing $s = \frac{1}{2}$ spin operators and derived an effective model for low-energy region assuming existence of a short-range spiral order. Then low-energy excitations are spinons and an emergent gauge field with local Z_2 gauge symmetry. We studied the effective gauge model for the quantum AF Heisenberg model by means of Monte Carlo (MC) simulations and obtained a phase diagram. There exist the spiral state, the paramagnetic (PM) dimer state, and the spin-liquid state in the phase diagram. These phases can be also labeled by the gauge dynamics, that is, Higgs, confinement, and Coulomb phases, respectively.

In the present paper, we shall continue the study in the previous work and investigate a closely related model, that is, an AF Heisenberg model on layered anisotropic triangular lattice. We are interested mostly in finite-T properties of the model. By using the Schwinger bosons and CP^1 path-integral methods, direct application of the MC simulations becomes possible *without* assuming any kind of (short-range) order. We discuss an advantage and reliability of the present numerical methods that are applicable for systems at finite T. Then we shall clarify the phase diagram of the model. Results obtained in this paper support the study in the previous paper.[6]

This paper is organized as follows. In Sec. II, we introduce models and give a derivation of the effective gauge-theory model. By using the Schwinger bosons, local U(1) gauge symmetry naturally appears. Then we discuss possible phases in the frustrated AF spin systems. Section III is devoted to numerical studies. We investigated phase structure of the model by calculating the internal energy, specific heat, spin correlation functions, etc. These numerical calculations show that there exist AF, PM, spiral, and spin-liquid phases. Detailed study on the critical behaviors between these phases is given. Section IV is devoted to summary and discussion.

II. QUANTUM AF SPIN MODEL, SCHWINGER BOSONS, CP^1 REPRESENTATION, AND GAUGE THEORY

In the present paper we study a spin-1/2 anisotropic AF Heisenberg model on a layered triangular lattice shown in Fig. 1. For simplicity, we first consider a 3D cubic lattice and then add diagonal links in the upper-right direction (1-2 direction) in 2D layers. The quantum Hamiltonian of the spin system is given as

$$H = J_1 \sum_{x,\mu} \hat{\mathbf{S}}_x \cdot \hat{\mathbf{S}}_{x+\mu} + J_2 \sum_{x} \hat{\mathbf{S}}_x \cdot \hat{\mathbf{S}}_{x+1+2}, \qquad (2.1)$$

where $\hat{\mathbf{S}}_x$ is the spin operator at site x and $\mu(= 1,2,3)$ is a direction index and also denotes unit vector in 3D lattice, whereas 1 and 2 are those of the 2D lattice. Therefore, the J_1 term in Eq. (2.1) is the 3D nearest-neighbor (NN) AF interaction, whereas the J_2 term is the next-nearest-neighbor (NNN) AF coupling in 2D layers. There exists an AF Néel order for $J_1 \gg J_2$ at low temperature (T), and it is expected that a quantum phase transition takes place as J_2 is increased.

In this paper, we investigate finite-T properties of the system (2.1) in detail. To this end, we employ the Schwinger-

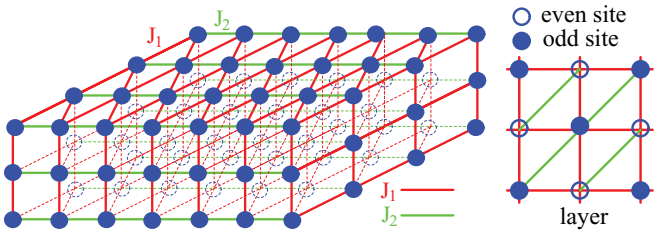

FIG. 1. (Color online) Three-dimensional layered lattice on which the spin models (2.1) are defined.

boson representation and the coherent-path-integral methods.[7] By means of these methods, numerical study of the system can be performed straightforwardly. In terms of the Schwinger bosons at site x, $\hat{a} = (\hat{a}_{x\uparrow}, \hat{a}_{x\downarrow})^t$ (where $\mathcal{O}^t$ denotes a transpose of the vector/matrix $\mathcal{O}$), the spin operator $\hat{\mathbf{S}}_x$ is expressed as

$$\hat{\mathbf{S}}_x = \tfrac{1}{2}\hat{a}_x^\dagger \vec{\sigma} \hat{a}_x, \tag{2.2}$$

where $\vec{\sigma}$ are the Pauli spin matrices. As the magnitude of the quantum spin is $\frac{1}{2}$, the physical states of the Schwinger bosons, $|\text{Phys}\rangle$, have to satisfy the following constraint at each site x,

$$\sum_{\sigma=\uparrow,\downarrow} \hat{a}_{x\sigma}^\dagger \hat{a}_{x\sigma} |\text{Phys}\rangle = |\text{Phys}\rangle. \tag{2.3}$$

We use the coherent-state path integral for the study of the system (2.1) expressed in terms of the Schwinger bosons. To this end, we introduce CP^1 variables $z_x = (z_{x\uparrow}, z_{x\downarrow})^t$ corresponding to $\hat{a}_{x\sigma}$, which satisfy the constraint

$$\sum_{\sigma=\uparrow,\downarrow} \bar{z}_{x\sigma} z_{x\sigma} = 1, \tag{2.4}$$

as required by Eq. (2.3).

Then the partition function Z is given by

$$\begin{aligned} Z &= \int [Dz]_{\text{CP}} \exp\left[\int_0^\beta d\tau A(\tau)\right], \\ A(\tau) &= -\sum_{x,\sigma} \bar{z}_{x\sigma} \partial_\tau z_{x\sigma} - H(\bar{z},z), \end{aligned} \tag{2.5}$$

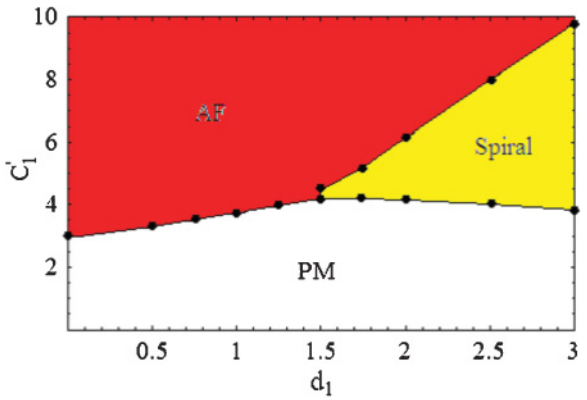

FIG. 2. (Color online) Obtained phase diagram for model S_2 with $c_2 = 0$. There are three phase transition lines, which separate AF, PM and spiral phases. All phase transitions are of second order. Locations of phase transition lines are determined by calculations of system size $L = 16$.

where τ is the imaginary time, $\beta = 1/(k_B T)$, $[Dz]$ denotes the path integral over CP^1 variables, and $H(\bar{z},z)$ is obtained from Eq. (2.1) by using Eq. (2.2). $H(\bar{z},z)$ in Eq. (2.5) is explicitly given as (up to an irrelevant constant)

$$\begin{aligned} H(\bar{z},z) &= \frac{J_1}{2}\sum_{x,\mu} |\bar{z}_x z_{x+\mu}|^2 + \frac{J_2}{2}\sum_x |\bar{z}_x z_{x+1+2}|^2 \\ &= -\frac{J_1}{2}\sum_{x,\mu} |\bar{z}_x \tilde{z}_{x+\mu}|^2 - \frac{J_2}{2}\sum_x |\bar{z}_x \tilde{z}_{x+1+2}|^2, \end{aligned} \tag{2.6}$$

where $\tilde{z}_x = (\bar{z}_{x\downarrow}, -\bar{z}_{x\uparrow})^t$, which is nothing but the time-reversal spinor of z_x, and we have used the fact that z_x and $\tilde{z}_x$ are an orthogonal and complete set of vectors in the CP^1 space. If one tries to numerically study the system (2.5) by means of the MC simulations, one immediately encounters difficulties in the important sampling procedure because the first term in the action $A(\tau)$ is pure imaginary. For $J_1 \gg J_2$, it is known that by integrating out the CP^1 variables z_x at all odd (or even) sites of the cubic lattice by assuming a short-range AF order, the resultant action has a quartic form of $z_{x\sigma}$ ($x \in$ even sites) and has a lower bound.[8] This calculation, however, cannot be applicable for the case $J_1 \sim J_2$ that we are interested in. Therefore, we take another way to avoid the imaginary term in $A(\tau)$; that is, we consider finite-T properties of the system (2.5) and ignore the imaginary-time dependence of variables z_x. The study of finite-T properties of the system is not only interesting itself but also gives an important insight into low-T properties of the system as it is expected that an ordered phase at finite T survives at lower T.[9]

Physical meaning of the above approximation is clarified by the following qualitative discussion on system of general boson field $\phi_{\vec{x}}$ at finite T. We consider the boson field $\phi_{\vec{x}}$ with Hamiltonian H_B in the continuum space for simplicity. The partition function Z_ϕ is given as

$$\begin{aligned} Z_\phi &= \int [d\phi] \exp\left[\int_0^\beta d\tau A_\phi(\tau)\right], \\ A_\phi(\tau) &= -\int dx \bar{\phi}_{\vec{x}}(\tau)\partial_\tau \phi_{\vec{x}}(\tau) - H_B(\bar{\phi},\phi). \end{aligned} \tag{2.7}$$

Then we Fourier decompose $\phi_{\vec{x}}(\tau)$ as

$$\phi_{\vec{x}}(\tau) = \sum_{n=-\infty}^{\infty} e^{i\omega_n \tau} \phi_{\vec{x},n}, \tag{2.8}$$

where $\omega_n = \frac{2\pi n}{\beta}$, and

$$\int_0^\beta d\tau \bar{\phi}_{\vec{x}}(\tau)\partial_\tau \phi_{\vec{x}}(\tau) = \sum_n (2\pi n i)\bar{\phi}_{\vec{x},n}\phi_{\vec{x},n}. \tag{2.9}$$

On the other hand,

$$\begin{aligned} &\int_0^\beta d\tau H_B(\bar{\phi}_{\vec{x}}(\tau), \phi_{\vec{x}}(\tau)) \\ &= \beta H_B(\bar{\phi}_{\vec{x},0}, \phi_{\vec{x},0}) + \beta H_1(\bar{\phi}_{\vec{x},0}, \phi_{\vec{x},0}, \bar{\phi}_{\vec{x},n\neq 0}, \phi_{\vec{x},n\neq 0}), \end{aligned} \tag{2.10}$$

where the first term $H_B(\bar{\phi}_{\vec{x},0}, \phi_{\vec{x},0})$ contains only the zero modes $\phi_{\vec{x},0}$, whereas the second term $H_1(\bar{\phi}_{\vec{x},0}, \phi_{\vec{x},0}, \bar{\phi}_{\vec{x},n\neq 0}, \phi_{\vec{x},n\neq 0})$ represents the interactions between the zero modes and nonzero modes $\phi_{\vec{x},n\neq 0}$, as well

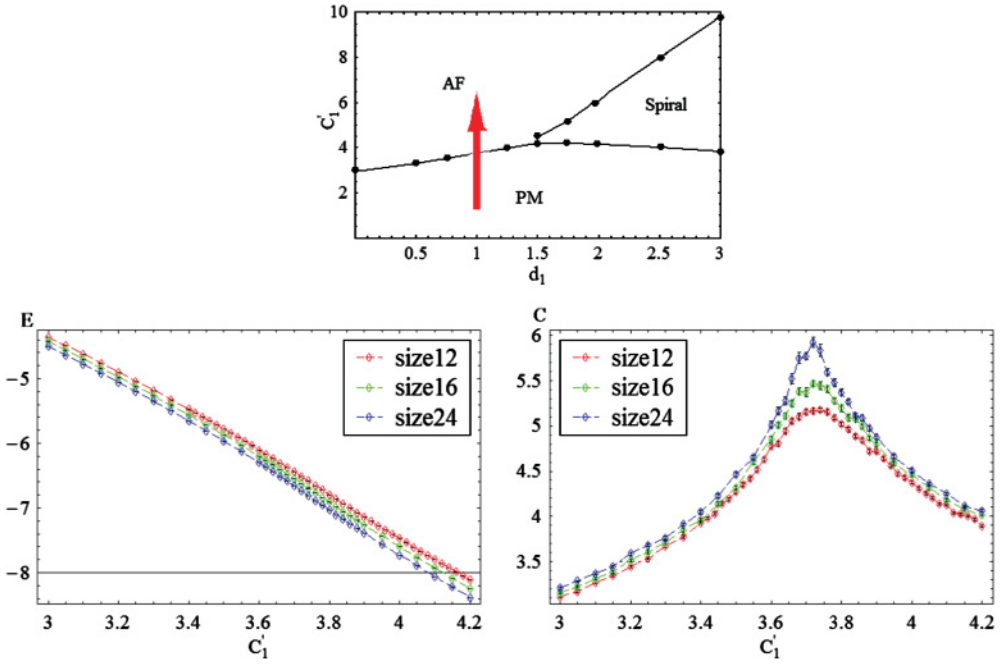

FIG. 3. (Color online) Phase transition from PM to AF phases for $d_1 = 1.0$. E exhibits no anomalous behavior, whereas C has a peak that develops as the system size is increased. By finite size scaling of C, it is verified that there exists a second-order phase transition at $c_1' \simeq 3.70$.

as the spatial derivative term of $\phi_{\vec{x},n\neq 0}$. The typical form of $H_1(\bar{\phi}_{\vec{x},0},\phi_{\vec{x},0},\bar{\phi}_{\vec{x},n\neq 0},\phi_{\vec{x},n\neq 0})$ is like

$$H_1 = \sum_{n\neq 0}\int dx \bar{\phi}_{\vec{x},0}\phi_{\vec{x},0}\bar{\phi}_{\vec{x},n}\phi_{\vec{x},n} + \cdots . \tag{2.11}$$

Effective action of the zero modes is obtained by integrating out the nonzero modes in Eq. (2.7):

$$\begin{aligned}\int [d\phi]\exp\left[\int_0^\beta d\tau A_\phi(\tau)\right] &= \int [d\phi_0] e^{-\beta H_B(\bar{\phi}_{\vec{x},0},\phi_{\vec{x},0})}\int [d\phi_{n\neq 0}]\exp\Bigg[-\sum_{n\neq 0}(2\pi n i)\\ &\times\bar{\phi}_{\vec{x},n}\phi_{\vec{x},n} - \beta H_1(\bar{\phi}_{\vec{x},0},\phi_{\vec{x},0},\bar{\phi}_{\vec{x},n\neq 0},\phi_{\vec{x},n\neq 0})\Bigg].\end{aligned} \tag{2.12}$$

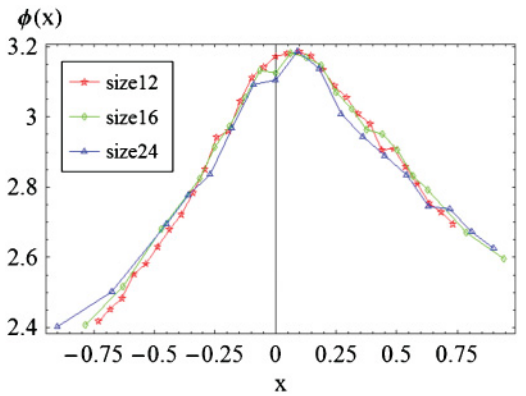

FIG. 4. (Color online) Scaling function $\phi(x)$ for the specific heat shown in Fig. 3. All data are fit by scaling function $\phi(x)$.

The Green function of $\phi_{\vec{x},n\neq 0}$ behaves as

$$\langle\bar{\phi}_{\vec{x},n\neq 0}\phi_{\vec{y},n\neq 0}\rangle \sim \exp\left[-\sqrt{\left(\frac{2\pi|n|T}{v}\right)^2 + m_\phi^2 v^2}|\vec{x}-\vec{y}|\right], \tag{2.13}$$

for $|\vec{x}-\vec{y}|\to\infty$, where v is the speed of bosonic excitation [for the spin wave $v = Ja$ (a = lattice spacing)] and m_ϕ is the energy gap of excitation. Equation (2.13) corresponds to the case of bosons with a relativistic dispersion but similar exponential damping behavior appears for bosons having non relativistic dispersion. Then integration over nonzero modes in Eq. (2.12) renormalizes $H_B(\bar{\phi}_{\vec{x},0},\phi_{\vec{x},0})$ but it is expected that this renormalization does not change drastically the structure of $H_B(\bar{\phi}_{\vec{x},0},\phi_{\vec{x},0})$ because of the behavior of the Green functions (2.13). At $T = 0$, the Green functions have only an algebraic decay in the case $m_\phi = 0$, and therefore nonlocal interactions generated by integration over nonzero modes may change the phase structure of the system and generate a new ordered state.[10] In any case, the renormalization by the nonzero modes $\phi_{\vec{x},n\neq 0}$ is more effective at lower T and it is physically expected that the renormalization enhances ordered states. Therefore, an ordered phase at finite T survives at lower T.[9]

In the above approximation, the partition function is given as

$$\begin{aligned} Z &= \int [Dz]_{\rm CP}\exp(-S_0),\\ S_0 &= -\frac{J_1\beta}{2}\sum_{x,\mu}|\bar{z}_x\tilde{z}_{x+\mu}|^2 + \frac{J_2\beta}{2}\sum_x|\bar{z}_x z_{x+1+2}|^2\\ &= -c_1\sum_{x,\mu}|\bar{z}_x\tilde{z}_{x+\mu}|^2 + d_1\sum_x|\bar{z}_x z_{x+1+2}|^2,\end{aligned} \tag{2.14}$$

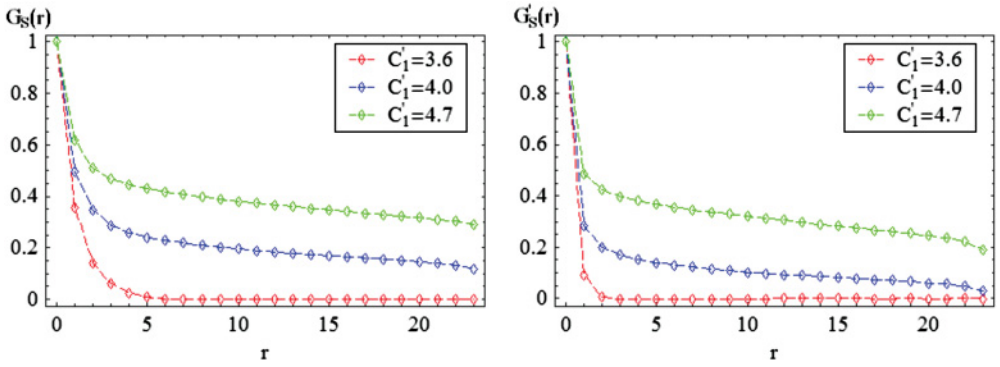

FIG. 5. (Color online) Spin correlation functions for $d_1 = 1.0$. The results indicate that there exists an AF long-range order at $c' = 4.0$ and 4.7, whereas at $c' = 3.6$ spin correlation decays quite rapidly because of nonexistence of long-range order. System size $L = 24$.

where $c_1 = \frac{J_1\beta}{2}$ and $d_1 = \frac{J_2\beta}{2}$. For later discussion, it is useful to slightly change the action S_0 in Eq. (2.14) as follows. We first rename CP[1] variables at odd sites of the cubic lattice as

$$z_x \to \bar{z}_x, \quad x \in \text{odd site}, \tag{2.15}$$

and introduce a gauge field $U_{x\mu}$ at link (x,μ) for the AF spin-pair channel. Then

$$S_1 = -c_1' \sum_{x,\mu} (\bar{z}_{x+\mu} U_{x\mu} z_x + \text{c.c.}) + d_1 \sum_x |\bar{z}_x z_{x+1+2}|^2. \tag{2.16}$$

A one-link integral over the gauge field $U_{x\mu} = e^{i\theta_{x\mu}}$ can be performed exactly,

$$\int \frac{d\theta_{x\mu}}{2\pi} \exp(c_1' \bar{z}_{x+\mu} U_{x\mu} z_x + \text{c.c.}) = \exp(\log I_0(c_1' |\bar{z}_{x+\mu} z_x|)), \tag{2.17}$$

where I_0 is the modified Bessel function. From the behavior of the modified Bessel function I_0, relation between the parameters c_1 and c_1' is obtained as follows:

$$c_1' \sim \begin{cases} c_1 & \text{for} \quad c_1 \gg 1, \\ (c_1)^{1/2} & \text{for} \quad c_1 \ll 1. \end{cases} \tag{2.18}$$

Action S_1 is invariant under the following *local gauge transformation*,

$$z_{x\sigma} \to z_{x\sigma} e^{i\Lambda_x}, \bar{z}_{x\sigma} \to \bar{z}_{x\sigma} e^{-i\Lambda_x}, \quad U_{x\mu} \to e^{i\Lambda_{x+\mu}} U_{x\mu} e^{-i\Lambda_x}, \tag{2.19}$$

where Λ_x is an arbitrary gauge-transformation parameter. In order to investigate the possibility of the appearance of a spin liquid with deconfined spinon excitations, study of the gauge dynamics and behavior of the gauge field $U_{x\mu}$ is important and necessary. As we show later, the two systems S_0 and S_1 have qualitatively the same phase structure.

We also add a plaquette term of the gauge field $U_{x\mu}$ to the action S_1 in Eq. (2.16) as

$$S_2 = -c_1' \sum_{x,\mu} (\bar{z}_{x+\mu} U_{x\mu} z_x + \text{c.c.}) + d_1 \sum_x |\bar{z}_x z_{x+1+2}|^2 - c_2 \sum_{x,\mu>\nu} U_{x\mu} U_{x+\mu,\nu} \bar{U}_{x+\nu,\mu} \bar{U}_{x\nu} + \text{c.c.}, \tag{2.20}$$

where the last plaquette term is the counterpart of the Maxwell term of the gauge field $\theta_{x\mu}$ in the continuum. It is obvious that by setting $c_2 = 0$ in S_2 (2.20), S_2 reduces to S_1 in Eq. (2.16).

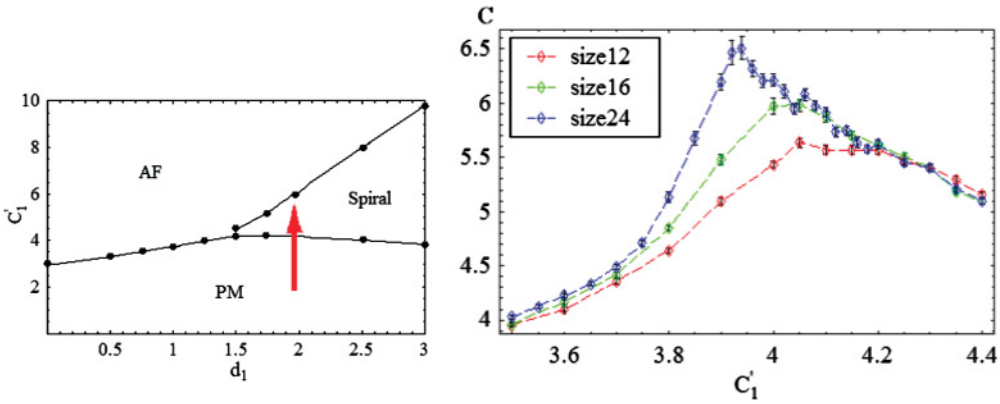

FIG. 6. (Color online) Phase transition from PM to spiral states for $d_1 = 2.0$. Total specific heat C has a peak that develops as L is increased. Finite-size scaling analysis verifies that this peak indicates a second-order phase transition.

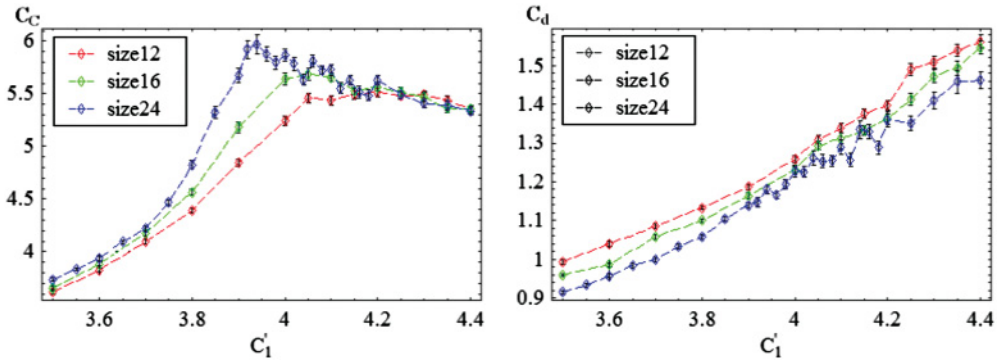

FIG. 7. (Color online) Specific heat of each term in action defined by Eq. (3.4) for $d_1 = 2.0$. Calculation of C_c shows that c_1 term in action fluctuates strongly at phase transition whereas calculation of C_d shows that d_1 term does not. This implies that appearance of spiral order influences NN spin pairs more strongly than pairs in diagonal links as c_1' is increased.

By integrating out the gauge field $U_{x,\mu}$ as

$$\int \prod \frac{d\theta_{x\mu}}{2\pi} \exp\left(c_1' \sum_{x,\mu} \bar{z}_{x+\mu} U_{x\mu} z_x + c_2 \sum_{x,\mu>\nu} U_{x\mu} U_{x+\mu,\nu} \bar{U}_{x+\nu,\mu} \bar{U}_{x\nu} + \text{c.c.} \right), \quad (2.21)$$

there appear the following terms in the effective action:

$$(c_1')^4 c_2 (\bar{z}_{x+\mu} z_x)(\bar{z}_{x+\mu+\nu} z_{x+\mu})(\bar{z}_{x+\nu} z_{x+\mu+\nu})(\bar{z}_x z_{x+\nu}) + \text{c.c.} + \cdots \propto (c_1')^4 c_2 (\hat{\mathbf{S}}_x \cdot \hat{\mathbf{S}}_{x+\mu})(\hat{\mathbf{S}}_{x+\nu} \cdot \hat{\mathbf{S}}_{x+\mu+\nu}) + \cdots, \quad (2.22)$$

which correspond to the ring-exchange terms of spins. Higher-order terms of c_2 correspond to nonlocal interactions between spins. Therefore, the action S_2 in Eq. (2.20) corresponds to the AF Heisenberg model with the ring-exchange terms besides the J_1 and J_2 terms in Eq. (2.1).

It should be noticed that the plaquette term is defined on the 3D cubic lattice, and therefore the induced ring-exchange interaction is 3D. The gauge field $U_{x\mu}$ is related to the original Schwinger-boson operators as

$$U_{x\mu} \sim \begin{cases} \hat{a}_{x+\mu\uparrow} \hat{a}_{x\downarrow} - \hat{a}_{x+\mu\downarrow} \hat{a}_{x\uparrow}, & x \in \text{odd site}, \\ \hat{a}^\dagger_{x+\mu\uparrow} \hat{a}^\dagger_{x\downarrow} - \hat{a}^\dagger_{x+\mu\downarrow} \hat{a}^\dagger_{x\uparrow}, & x \in \text{even site}; \end{cases} \quad (2.23)$$

that is, $U_{x\mu}$ corresponds to creation and destruction operators of spin-singlet bond at sites x and $x+\mu$. Therefore, the c_2 terms in the action S_2 (2.20) flip pairs of parallel NN spin-singlet bonds and enhance the appearance of the resonating-valence-bond (RVB) liquid.[11]

From the previous studies,[6,12] phase structure of the quantum spin models corresponding to S_2 in Eq. (2.20) is expected as follows.

(i) For $d_1 = c_2 = 0$, a phase transition from a PM state to the Néel state with AF long-range order takes place as c_1 is increased.[13] In a gauge-fixed formalism, the AF Néel state corresponds to the state in which $\langle z_x \rangle \neq 0$ and $\langle U_{x\mu} \rangle \simeq 1$.

(ii) As the value of d_1 is increased in the AF phase, a spiral state appears at some critical value of $d_{1c}(c_1)$.[14] In the spiral state, z_x is parameterized as

$$z_x = \frac{1}{\sqrt{2}} (e^{i\omega x} v_x + e^{-i\omega x} \tilde{v}_x),$$

where ω is a constant, and the condensation of smoothly varying field v_x takes place, $\langle v_x \rangle \neq 0$.

(iii) Furthermore, as the value of c_2 is increased, a spin-liquid state with a deconfined spinon appears. In the spin-liquid phase, $\langle z_x \rangle = \langle v_x \rangle = 0$ and the gauge dynamics of $U_{x\mu}$ is in the Coulomb phase. A gapless gauge boson appears as a low-energy excitation coupled to spinons.

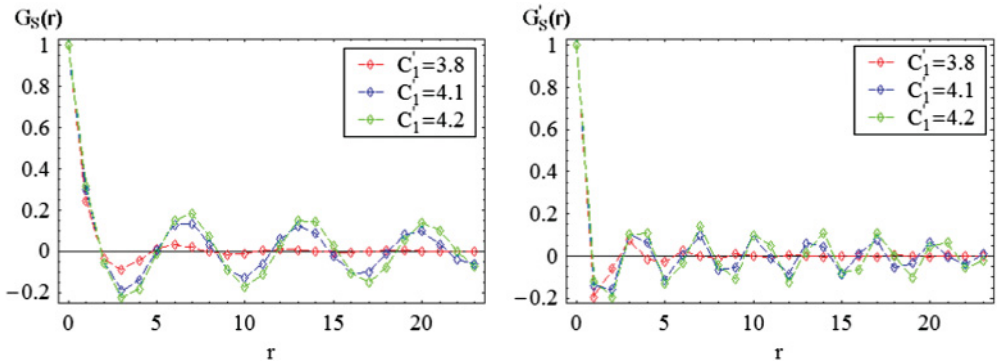

FIG. 8. (Color online) Spin correlations in PM and spiral states for $d_1 = 2.0$. For $c_1' = 4.1$ and 4.2, there is a LRO close to 120°-Néel order. On the other hand, calculation for $c_1' = 3.8$ indicates that spin correlation exhibits short-range spiral order. We particularly call this state the tilted-dimer state, though it is a part of PM phase. Please remember that the direction of odd-site spins has been reversed.

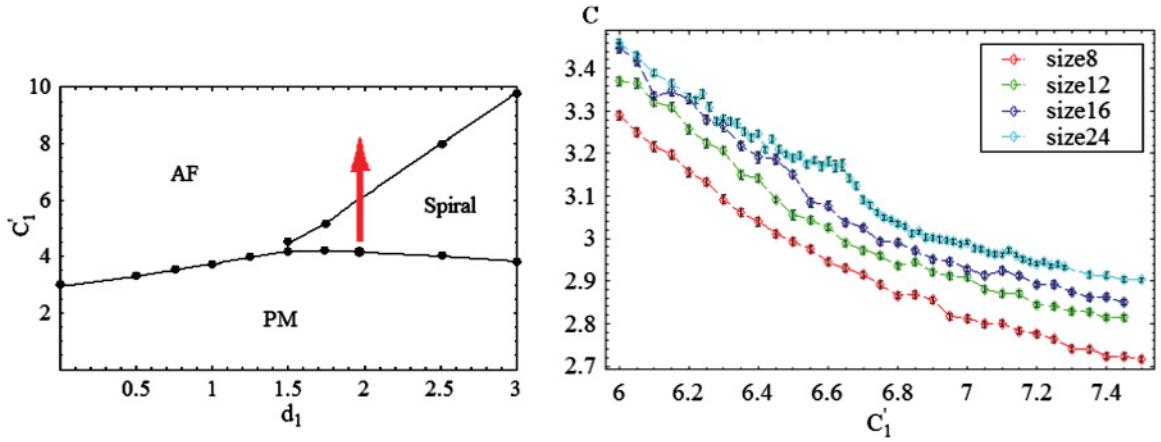

FIG. 9. (Color online) Phase transition from the spiral to AF phases for $d_1 = 2.0$. Total specific heat C for $d_1 = 2.0$ exhibits only weak anomalous behavior at spiral to AF phase transition $c_1' \simeq 6.65$.

In the following section, we show the results of studies on the phase diagram and physical properties of the models S_2 in Eq. (2.20) and S_0 in Eq. (2.14), which support qualitatively the above expectation. As mentioned in the Introduction, the experiments for frustrated quantum magnet Cs_2CuCl_4 observed the spiral state and the deconfined spin-liquid state.[2,3] Experimental results suggest a crossover in nature of the excitations from spin-1 spin waves at low energies to deconfined spin-1/2 spinons at medium to high energies. Furthermore, $EtMe_3Sb[Pd(dmit)_2]_2$, which is studied intensively these days, is closely related to the present model. Therefore, results in this paper are relevant to these materials.

III. NUMERICAL STUDIES

A. $c_2 = 0$ case

In the previous section, we derived the effective models of the $CP^1 + U(1)$ gauge variables from the AF Heisenberg model on layered triangular lattice. In this section we show results of the numerical study of the models obtained by means of the MC simulations. We employed the *free boundary condition* in the 1-2 plane as the system may have an incommensurate spiral order with the layered structure.

We first consider the case with $c_2 = 0$. We investigated phase structure of the model S_2 by calculating the internal energy E and the specific heat C for various values of c_1' and d_1,

$$E = \frac{1}{L^3}\langle S_2 \rangle, \quad C = \frac{1}{L^3}\langle (S_2 - \langle S_2 \rangle)^2 \rangle, \tag{3.1}$$

where L is the system size of the 3D lattice. In the practical calculation, we employed the local update by the standard Metropolis algorithm for the total system with size $(2 + L + 2) \times (2 + L + 2) \times L$ and performed measurement of physical quantities in the central $L \times L \times L$ subsystem.[15]

We have found that E exhibits no anomalous behaviors, whereas C exhibits singular behaviors that indicate the existence of second-order phase transitions as c_1' and d_1 are varied. Observed phase transition lines in the d_1-c_1' plane are shown in Fig. 2.

We first consider the PM-AF phase transition. In Fig. 3, we show E and C as functions of c_1' for $d_1 = 1.0$. It is obvious that E exhibits no anomalous behavior, whereas C has a peak at $c_1' \simeq 3.75$ and the peak develops as the system size is increased. This behavior of C indicates a second-order phase transition. To verify this observation, we perfomed the

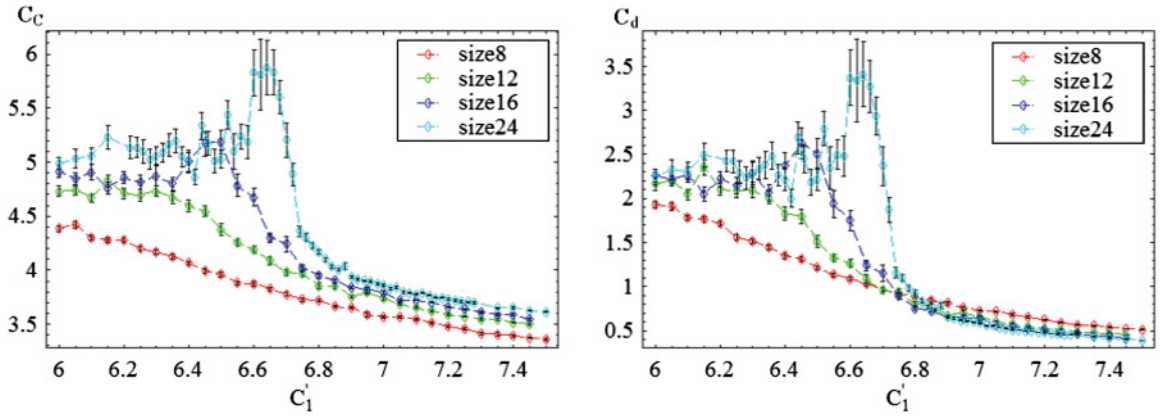

FIG. 10. (Color online) Specific heat of each term for spiral to AF phases transition for $d_1 = 2.0$. Both C_c and C_d exhibit a sharp peak at $c_1' \simeq 6.65$ as system size is increased.

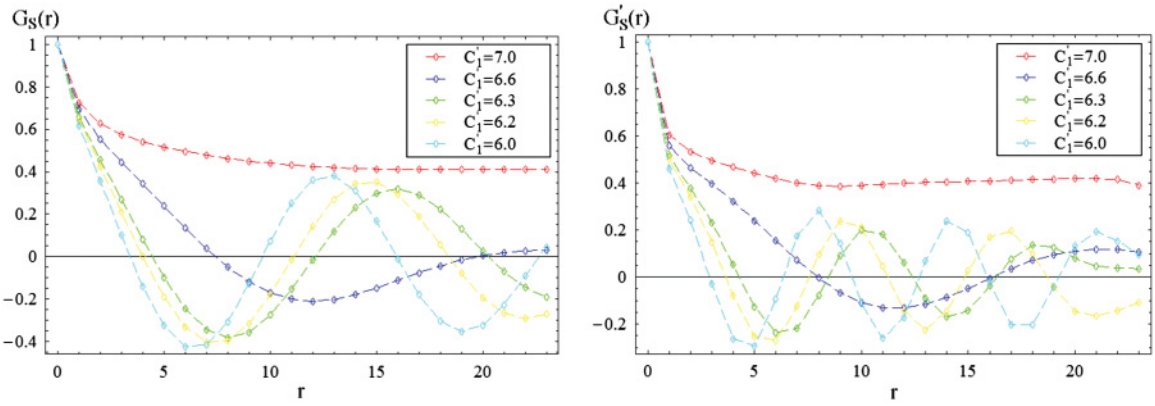

FIG. 11. (Color online) Spin correlation in spiral and AF states for $d_1 = 2.0$. It gradually changes from spiral to AF orders as c_1' is increased.

following finite-size scaling (FSS) analysis for the specific heat,

$$C_L(\epsilon) = L^{\sigma/\nu}\phi(L^{1/\nu}\epsilon), \tag{3.2}$$

where C_L is the specific heat of system size L, and $\epsilon \equiv (c_1' - c_{1\infty}')/c_{1\infty}'$ with $c_{1\infty}'$ (the critical coupling for $L \to \infty$), and we estimated the critical exponents as $\nu = 1.1$ and $\sigma = 0.22$ and the critical coupling $c_{1\infty}' = 3.70$. The resultant scaling function $\phi(x)$ is shown in Fig. 4.

In order to understand the physical meaning of each phase, we investigated correlation functions of spins that are given as

$$G_S(r) = \frac{1}{2}\sum_{j=1,2}\langle \mathbf{n}_x \cdot \mathbf{n}_{x+jr}\rangle, \quad G_S'(r) = \langle \mathbf{n}_x \cdot \mathbf{n}_{x+(1+2)r}\rangle, \tag{3.3}$$

where $\mathbf{n}_x = (\bar{z}_x \vec{\sigma} z_x)$. Numerically obtained results are shown in Fig. 5. At $c_1' = 3.6$, the correlation functions have no long-range order (LRO). On the other hand, at $c_1' = 4.0$ and 4.7, they exhibit AF LRO. (Please recall that we have changed variables $z_x \to \tilde{z}_x$, $x \in$ odd site.) From this result, we conclude that transition from the PM to AF phases takes place at $c_1' \simeq 3.70$.

We turn to the phase transition from the PM to spiral states, as shown in Fig. 6. For $d_1 = 2.0$, calculation of the total specific heat C as a function of c_1' is shown in Fig. 6. We also measured the specific heat of each term of the action, which is defined similarly to C in Eq. (3.1), in order to see the physical meaning of the phase transition:

$$C_c = \frac{1}{L^3}\langle (S_c - \langle S_c\rangle)^2\rangle, \qquad C_d = \frac{1}{L^3}\langle (S_d - \langle S_d\rangle)^2\rangle, \tag{3.4}$$

where

$$S_c = -c_1' \sum_{x,\mu} (\bar{z}_{x+\mu} U_{x\mu} z_x + \text{c.c.}), \qquad S_d = d_1 \sum_x |\bar{z}_x z_{x+1+2}|^2 \tag{3.5}$$

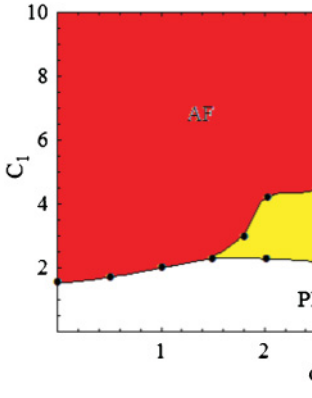

FIG. 12. (Color online) Phase diagram of model S_0. There are three phases, AF, PM, and spiral, as in the model S_2. All phase transition lines are of second order.

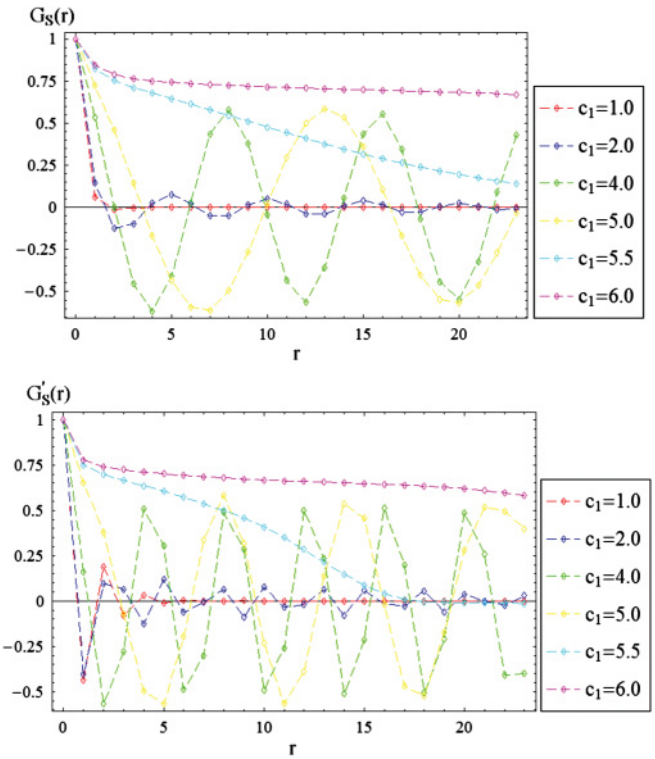

FIG. 13. (Color online) Spin correlation functions in model S_0 for $d_1 = 3.0$.

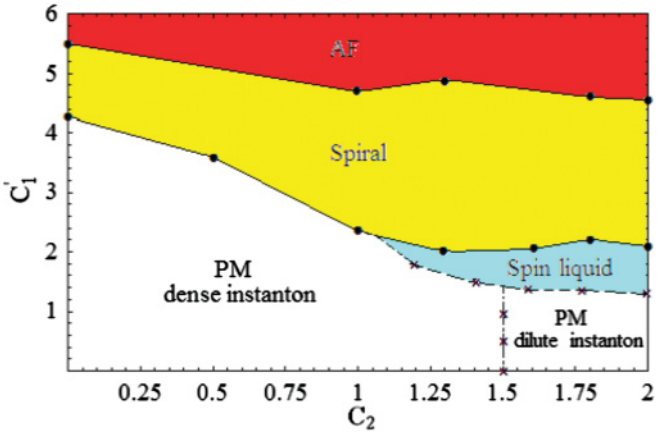

FIG. 14. (Color online) Phase diagram in the c_2-c_1' plane for $d_1 = 2.0$. The spin-liquid phase appears in the vicinity of PM (tilted-dimer) and spiral phases.

(see Fig. 7). From these results, it is obvious that a second-order phase transition from the PM to spiral states takes place at $c_1' \simeq 3.9$. It is interesting to see that the c_1' term of the action tends to fluctuate strongly at the phase transition point but the d_1 term does not.

We measured the spin correlations at $c_1' = 3.8, 4.1$, and 4.2. The results are shown in Fig. 8. It is obvious that at $c_1' = 3.8$ the spin does not have a LRO, whereas at $c_1' = 4.1$ and 4.2 it has a spiral LRO. One should notice, however, that at $c_1' = 3.8$ the spin correlation has a short-range spiral order,

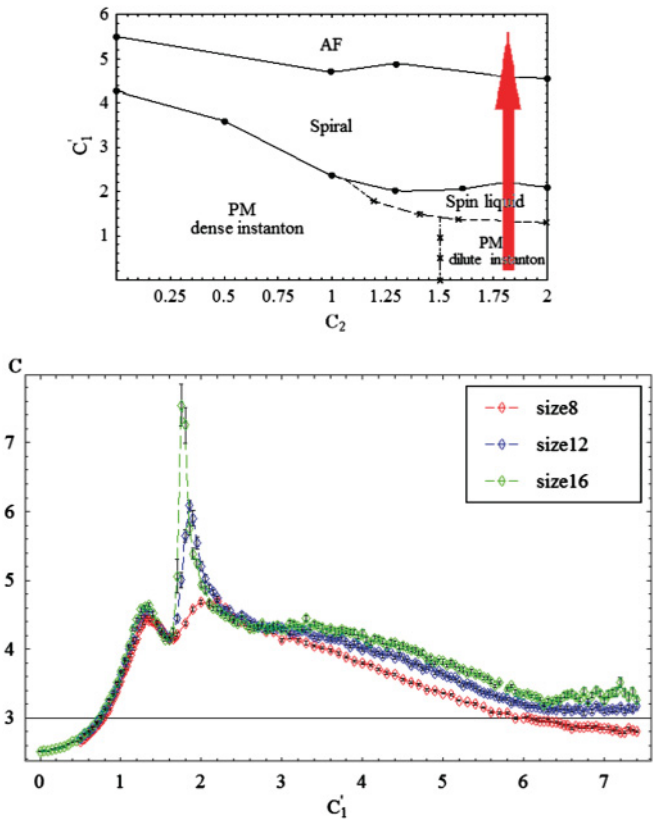

FIG. 15. (Color online) C as a function of c_1' for $c_2 = 1.8$ and $d_1 = 2.0$. There are two peaks at $c_1' \simeq 1.4$ and 1.8.

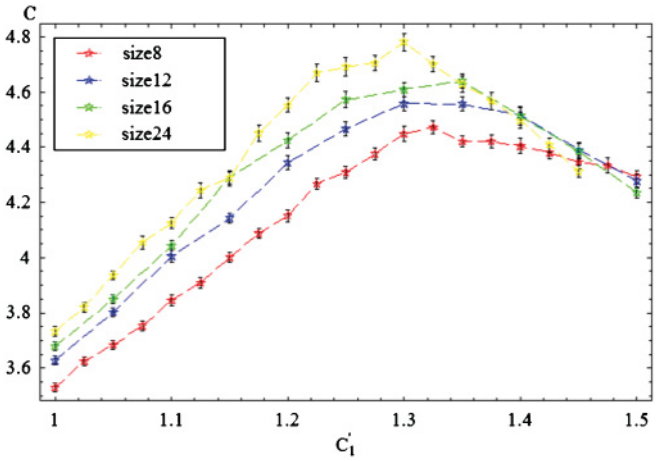

FIG. 16. (Color online) Detailed calculation of C as a function of c_1' for $c_2 = 1.8$ and $d_1 = 2.0$. A peak does not develop as system size is increased.

and therefore we call this "phase" a *tilted-dimer state*, though there is no sharp phase boundary between the ordinary PM with short-range AF order (at $d_1 \ll 1$) and a tilted-dimer state with short-range spiral order. This observation supports our previous study of the AF magnets on anisotropic triangular lattice assuming short-range spiral order.[6] We also measured the spin correlation in the interlayer direction in the spiral state and found that it has an ordinary AF correlation, as expected.

We calculated the specific heat and spin correlations for various values of the parameters c_1' and d_1 and have obtained a phase transition line that separates the PM and spiral phases.

Finally, let us turn to the spiral-AF phase transition (see Fig. 9). We show calculations of C and the specific heat of c_1' and d_1 terms (see Figs. 9 and 10). It is obvious that the total specific heat C exhibits only very weak anomalous behavior but C_c and C_d both show a sharp peak at $c_1' \sim 6.7$ as the system size is increased. From this result, we conclude that the transition from the spiral to AF phases is of second order.

It is also interesting to see how the spin correlation changes from the spiral to AF phases. Results in Figs. 11 show that the spin correlation gradually changes from the spiral order to the AF order.

We also numerically studied the original model S_0 in Eq. (2.14) and obtained similar results to those of model S_2. The obtained phase diagram is shown in Fig. 12, and spin correlation functions in Fig. 13. Phase transitions are of second order and spin-correlation functions have similar behavior to those of S_2.

Result for the spiral state obtained in the present subsection obviously means that the 120°-Néel state is realized in each layer for the case of the isotropic triangular case $J = J'$. This result is in good agreement with the previous study on the AF Heisenberg model on isotropic triangular lattice at $T = 0$.[16] On the other hand, some of the previous study on the anisotropic AF Heisenberg model on a 2D triangular lattice at $T = 0$ suggested the existence of spin-liquid phases.[17] In the present model, which describes physics of AF magnets on a layered anisotorpic triangular lattice, the results obtained in this section show that it does not exist. The spatial dimension of the systems may play an important role for the existence of

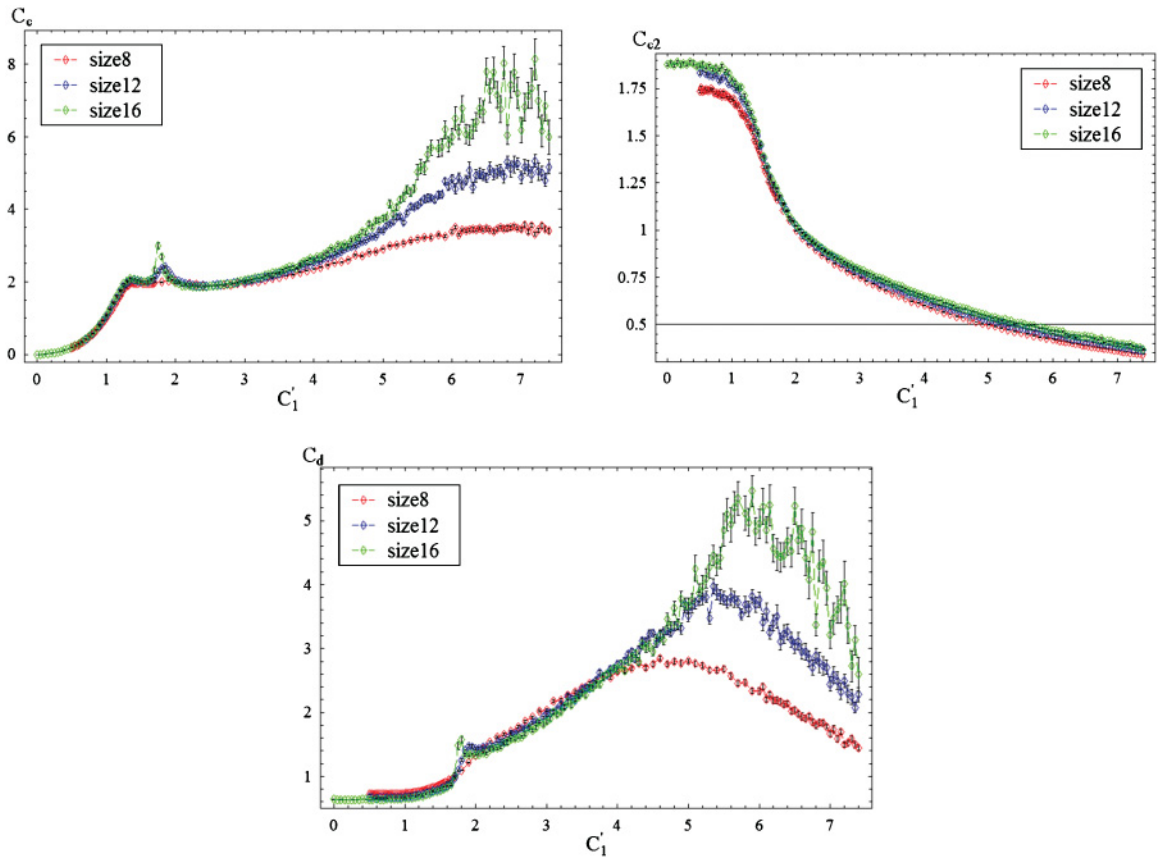

FIG. 17. (Color online) Specific heat of each term in action for $c_2 = 1.8$ and $d_1 = 2.0$. Behaviors of C_c, C_d, and C_{c2} indicate the existence of two phase transitions as $c_1' \simeq 1.8$ and $c_1' \simeq 5.5$, respectively.

the spin-liquid phase. In order to address the possibility of the spin-liquid phase in the present 3D model, we study the effect of the plaquette term of the emergent gauge field $U_{x\mu}$ in the following section.

B. $c_2 > 0$ case

In this section, we study the effects of the plaquette c_2 term in the action S_2. For the $c_2 = 0$ case, we found that there exist three phases, that is, the AF, spiral, and PM phases. It is expected that the gauge dynamics in both the AF and the spiral phases is in the Higgs phase as the condensation of the spinon field z_x suppresses fluctuations of the gauge field $U_{x\mu}$. Low-energy excitations are gapless spin waves in both phases. On the other hand, in the PM phase, it is known that the confinement phase is realized and low-energy excitations are the *bound state of the spinons* such as a spin triplet $(\bar{z}_x \vec{\sigma} z_x)$ because of the strong fluctuations of $U_{x\mu}$.

As explained in Sec. II, another possible phase in the quantum spin systems is the spin-liquid phase. In that phase, there exist no LROs, whereas low-energy excitation is the *deconfined spinon* z_x. This means that in the spin liquid only small fluctuations of the gauge field $U_{x\mu}$ are realized and the gauge dynamics is in the Coulomb phase. Knowledge of the gauge field theory suggests that such a spin-liquid phase may be realized by turning on the plaquette c_2 term because this term suppresses large fluctuations of the gauge field.[18] In the previous study on the Z_2 gauge model of the spiral and spin-liquid phases,[6] we found that the deconfined spin-liquid phase is realized in the vicinity of the spiral and tilted-dimer states. In the present paper, we show the results of study on the U(1) gauge model S_2 in the c_1'-c_2 parameter plane with the value of d_1 fixed.

We first show the phase diagram obtained by the MC simulations for $d_1 = 2.0$ in Fig. 14. The reason for choosing this value of d_1 is that the spiral and tilted-dimer states appear as the value of c_1' is varied for $c_2 = 0$. As shown in Fig. 14, there exists a crossover line emanating from the point $(c_2 \simeq 1.5, c_1 = 0)$ in the vertical direction. This crossover line separates dense and dilute instanton regions, whereas both regions belong to the confinement phase of the U(1) gauge model in 3D. Besides the crossover line, there exist two sharp second-order phase transition lines emanating from $(c_2 = 0, c_1' = 4.2)$ and $(c_2 = 0, c_1' = 5.5)$. As shown in Fig. 14, these are the spiral and AF phase transition lines, respectively. We also found another "transition line" emanating from $(c_2 \simeq 1.05, c_1' \simeq 2.2)$, which we identify as a crossover to the spin-liquid phase.

We show the total specific heat C as a function of c_1' for $c_2 = 1.8$ and $d_1 = 2.0$ in Fig. 15. There are two peaks at $c_1' \simeq 1.4$ and 1.8, and the second peak at $c_1' \simeq 1.8$ develops as the system size is increased, indicating a second-order phase transition. By FSS analysis, the critical exponent ν is estimated as $\nu = 0.75$ and the critical coupling for $L \to \infty$ as $c_{1\infty}' = 1.67$.

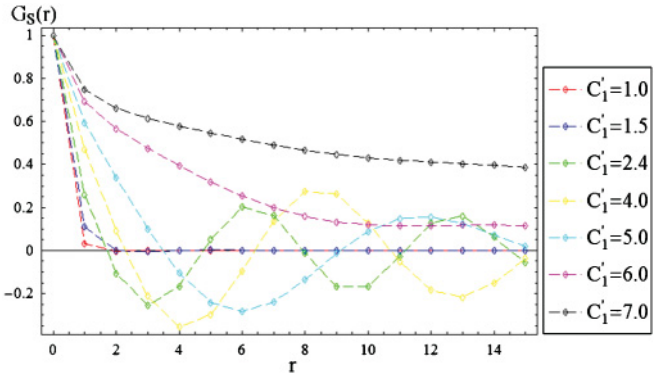

FIG. 18. (Color online) Spin correlation function for various values of c_1' ($c_2 = 1.8$ and $d_1 = 2.0$).

Calculation of the spin correlation given later shows that it is the phase transition to the spiral state. On the other hand, the first peak at $c_1' \simeq 1.4$ does not develop as the system size is increased. More detailed calculation is shown in Fig. 16. There exists small system-size dependence, but we think that this size dependence comes from the free-boundary condition that we took for the calculation.

It is useful to see how specific heat of each term behaves (see Fig. 17). The specific heat of the c_2 term C_{c2}, which is defined similarly to C_c and C_d, is a decreasing function of c_1' and changes its behavior at $c_1' \simeq 1.4$. On the other hand, the specific heats of the c_1' term and d_1 term both have peaks at $c_1' \simeq 1.8$ and $c_1' \simeq 5.5$ and these peaks develop as the system size is increased. This result suggests that there is a second-order phase transition at $c_1' \simeq 5.5$ besides that at $c_1' \simeq 1.8$.

It is important to see how the spin correlation function behaves and to verify properties of each phase observed by the measurement of C. Obtained results of the spin correlation for $c_2 = 1.8, d_1 = 2.0$ are shown in Fig. 18. At $c_1' = 1.0$ and 1.5, there exists no LRO, whereas at $c_1' = 2.4, 4.0$, and 5.0 the LR spiral order appears. Furthermore, at $c_1' = 6.0$, the spin correlation shows the AF LRO. All the above results verify the phase diagram shown in Fig. 14

In order to investigate the gauge dynamics, it is useful to study instanton (monopole) density ρ, which measures magnitude of topologically nontrivial fluctuations of the gauge field $U_{x\mu}$. $\rho(x)$ is defined as follows for the gauge field configuration $U_{x,\mu} = e^{i\theta_{x,\mu}}$.[12,19] First we consider the magnetic flux $\Theta_{x,\mu\nu}$ penetrating plaquette $(x, x+\mu, x+\mu+\nu, x+\nu)$:

$$\Theta_{x,\mu\nu} = \theta_{x,\mu} + \theta_{x+\mu,\nu} - \theta_{x+\nu,\mu} - \theta_{x,\nu}, \quad (-4\pi \leqslant \Theta_{x,\mu\nu} \leqslant 4\pi). \tag{3.6}$$

We decompose $\Theta_{x,\mu\nu}$ into its integer part $n_{x,\mu\nu}$, which represents the Dirac string (vortex line), and the remaining part $\tilde{\Theta}_{x,\mu\nu}$,

$$\Theta_{x,\mu\nu} = 2\pi n_{x,\mu\nu} + \tilde{\Theta}_{x,\mu\nu}, \quad (-\pi < \tilde{\Theta}_{x,\mu\nu} \leqslant \pi). \tag{3.7}$$

Then instanton density $\rho(x)$ at the cube around the site $x + \frac{\hat{1}}{2} + \frac{\hat{2}}{2} + \frac{\hat{3}}{2}$ of the dual lattice is defined as

$$\rho(x) = -\frac{1}{2}\sum_{\mu\nu\lambda} \epsilon_{\mu\nu\lambda}(n_{x+\mu,\nu\lambda} - n_{x,\nu\lambda})$$

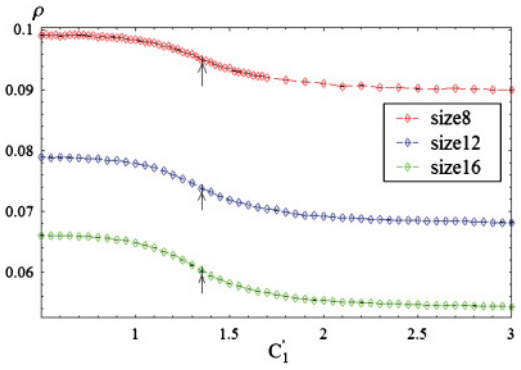

FIG. 19. (Color online) Instanton density as a function of c_1' ($c_2 = 1.8$ and $d_1 = 2.0$). Arrows indicate location of crossover observed by calculation of C. Small value of ρ means that fluctuations of gauge field $U_{x,\mu}$ are suppressed.

$$= \frac{1}{4\pi}\sum_{\mu\nu\lambda} \epsilon_{\mu\nu\lambda}(\tilde{\Theta}_{x+\mu,\nu\lambda} - \tilde{\Theta}_{x,\nu\lambda}), \tag{3.8}$$

where $\epsilon_{\mu\nu\lambda}$ is the antisymmetric tensor.

In Fig. 19, we show the calculation of

$$\rho = \frac{1}{L^3}\sum_x |\rho(x)|.$$

As the gauge dynamics is already in the dilute-instanton region of the confinement phase for $c_1' = 0$, the value of ρ is small, but it decreases at $c_1' \simeq 1.4$, and its behavior becomes clear as the system size is increased. This result indicates that the region between two peaks at $c_1' = 1.4$ and 1.8 corresponds to the "deconfined Coulomb phase." In this phase, the gapless gauge boson $\theta_{x\mu}$ appears as a low-energy excitation besides the deconfined spinons.

The global phase diagram in Fig. 14 is consistent with that of the Z_2 spin-liquid model obtained in Ref. 6. In the Z_2 model, however, the phase transition from spiral phase to PM phase is of first order and there exists a sharp phase boundary between spin-liquid and PM phases. Anyway, results obtained in this paper support discussions in term of Z_2 models for frustrated quantum AF magnets at $T = 0$.

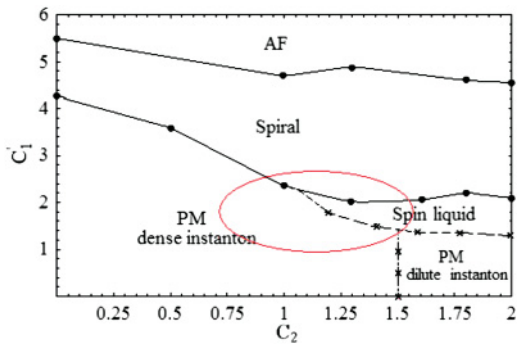

FIG. 20. (Color online) Circled region of the phase diagram was studied in the previous paper in terms of gauge theories with local Z_2 gauge symmetry (see Ref. 6). The results obtained in Ref. 6 and the present paper show that there exist the PM-tilted-dimer, spiral, and deconfined spin-liquid phases in the AF magnets on a triangular lattice at low T.

IV. SUMMARY

In this paper we have studied the phase structure of the AF spin model on a layered anisotropic triangular lattice. We used the Schwinger bosons for representing quantum spins and also employed the coherent-state path integral methods. We focused on finite-T phase diagram and investigated it by means of the MC simulations. We calculated the internal energy, specific heat, and spin correlation functions. In the absence of the c_2 term, we found that there exist three phases, that is, AF, PM, and spiral phases. All phase transitions between them are of second order.

Then we turned on the c_2 term and investigated if the deconfined spin-liquid phase appears. Calculations of the specific heat and instanton density show that there exists deconfined spin liquid in the vicinity of the spiral and tilted dimer states. This result is in good agreement with the results of our previous study[6] in which we assumed a short-range spiral order and focused on the region in the phase diagram shown in Fig. 20. However, the present study indicates that there is not a sharp phase boundary between the tilted-dimer state and spin liquid; that is, this "transition" is a crossover. At very low T, it is possible that this crossover changes to a genuine phase transition as the imaginary time plays a role of another dimension.

It is intriguing to notice that all of the observed phases in the present model exist in an effective field theory of U(1) Chern-Simons gauge fields that describe frustrated quantum AF magnets in 2D and at $T = 0$.[20] In that field theory, quasiexcitations are spinons and visons, which have mutual semionic statistics. Chern-Simon theory is quite useful to describe these excitations in 2D. Though there is no direct connection between Chern-Simons theory and the present 3D model, it is interesting to investigate possible relations between them.

It is also very interesting to study how hole doping changes the observed phase diagrams and how doped holes behaves in various magnetic phases. This problem is under study and we hope to report the results in a future publication.

ACKNOWLEDGMENT

This work was partially supported by Grant-in-Aid for Scientific Research from Japan Society for the Promotion of Science under Grant No. 20540264.

---

*Present address: Department of Applied Physics, Osaka University, Suita, Osaka 565-0871, Japan.

[1]See for example, S. Sachdev, Nat. Phys. **4**, 173 (2008); L. Balents, Nature (London) **464**, 199 (2010), and references cited therein.

[2]R. Coldea, D. A. Tennant, A. M. Tsvelik, and Z. Tylczynski, Phys. Rev. Lett. **86**, 1335 (2001).

[3]R. Coldea, D. A. Tennant, and Z. Tylczynski, Phy. Rev. B **68**, 134424 (2003).

[4]Y. Qi, C. Xu, and S. Sachdev, Phys. Rev. Lett. **102**, 176401 (2009).

[5]M. Yamashita, N. Nakata, Y. Senshu, M. Nagata, H. M. Yamamoto, R. Kato, T. Shibauchi, and Y. Matsuda, Science **328**, 1246 (2010); T. Itou, A. Oyamada, S. Maegawa, and R. Kato, Nat. Phys. **6**, 673 (2010).

[6]K. Nakane, A. Shimizu, and I. Ichinose, Phys. Rev. B **80**, 224425 (2009).

[7]See, for example, G. Misguich, in *Exact Methods in Low-dimensional Statistical Physics and Quantum Computing*, edited by J. Jacobsen, S. Ouvry, V. Pasquier, D. Serban, and L. F. Cugliandolo, Lecture Notes of the Les Houches Summer School, LXXXIX, 2008 (Oxford University Press, Oxford, 2010).

[8]I. Ichinose and T. Matsui, Phys. Rev. B **45**, 9976 (1992).

[9]See, for example, K. Aoki, K. Sakakibara, I. Ichinose, and T. Matsui, Phys. Rev. B **80**, 144510 (2009); K. Sawamura, T. Hiramatsu, K. Ozaki, I. Ichinose, and T. Matsui, *ibid.* **77**, 224404 (2008).

[10]For phase structure of nonlocal field theory, see G. Arakawa, I. Ichinose, T. Matsui, and K. Sakakibara, Phys. Rev. Lett. **94**, 211601 (2005); G. Arakawa, I. Ichinose, T. Matsui, K. Sakakibara, and S. Takashima, Nucl. Phys. B **732**, 401 (2006).

[11]P. W. Anderson, Science **235**, 1196 (1987).

[12]S. Takashima, I. Ichinose, and T. Matsui, Phys. Rev. B **72**, 075112 (2005).

[13]See for example, A. Auerbach, *Interacting Electrons and Quantum Magnetism* (Springer-Verlag, New York, 1994).

[14]J. Merino, R. H. McKenzie, J. B. Marston, and C. H. Chung, J. Phys. Condens. Matter **11**, 2965 (1999).

[15]N. Metropolis, A. W. Rosenbluth, M. N. Rosenbluth, A. M. Teller, and E. Teller, J. Chem. Phys. **21**, 1087 (1953).

[16]See, for example, S. R. White and A. L. Chernyshev, Phys. Rev. Lett. **99**, 127004 (2007), and references therein.

[17]S. Yunoki and S. Sorella, Phys. Rev. B **74**, 014408 (2006); D. Heidarian, S. Sorella, and F. Becca, *ibid.* **80**, 012404 (2009).

[18]J. B. Kogut, Rev. Mod. Phys. **51**, 659 (1979).

[19]T. A. DeGrand and D. Toussaint, Phys. Rev. D **22**, 2478 (1980).

[20]C. Xu and S. Sachdev, Phys. Rev. B **79**, 064405 (2009).